J Solid State Electrochem (2014) 18:3081–3090
DOI 10.1007/s10008-014-2422-2

ORIGINAL PAPER

Synthesis of ZrO_2 nanotubes in inorganic and organic electrolytes by anodic oxidation of zirconium

Michał Stępień · Piotr Handzlik · Krzysztof Fitzner

Received: 12 November 2013 / Revised: 31 January 2014 / Accepted: 2 February 2014 / Published online: 15 April 2014

Abstract Present work reports on the results of the electrochemical growth of self-ordered zirconia nanotubes formed in aqueous Na_2SO_4+HF and nonaqueous electrolytes with glycerol addition. Anodization process was carried out in this inorganic water-based mixture with constant pH=2.5 and in the voltage range from 5 to 60 V. Similar experiments were repeated in an organic glycerol-based electrolyte with the voltage equal to 20 V and with variable glycerol concentration. All experiments were conducted at constant room temperature. The tube diameter dependence on the voltage of anodization process in an inorganic electrolyte was derived. It was found that when glycerol addition to water electrolyte was used, it takes more time to produce long zirconia nanotubes. However, they do not collapse as the similar structure of the same length formed in aqueous electrolyte.

Keywords Anodization · ZrO_2 nanotubes · Electron microscopy · Morphology · Fabrication parameter

Introduction

During the anodization process carried out in solutions containing fluoride ions, valve metals and their alloys can form highly self-ordered arrays of nanotubes, nanopores, or nanorods on their surface, made up of their oxides. For the first time, the formation of these nanostructures has been observed on Al [1] and Ti [2, 3]. Very interesting chemical and physical properties of these oxides such as high chemical stability of the films, large surface area, catalytic properties, dielectric constant, and useful energy range of the band gap stimulated the attempts to obtain similar nanostructures on other metals like Zr [4–7] and Nb [8–10]. The possibility of handling these structures on atomic or molecular level opens the way for design and production of the systems on a nanometer scale, which is a base for nanotechnology development.

Since zirconium and its oxide are very promising materials to be used for implants [11, 12], protective coating for optical devices [13], and oxygen sensor [14, 15] in catalysis and they can be used as photocatalysts in environmental cleaning applications [16, 17], attempts have been made to determine the conditions of the controlled zirconium oxide layer growth. Especially, in the form of nanotubes, with high surface area, zirconia may find applications in gas sensors [18] and fuel cells [19] as catalysts or catalyst support [17, 20]. Activation towards improved photocatalytic activity may be achieved by decoration of the surface with silver nanoparticles (NPs). Such materials can enhance the efficiency of solar radiation conversion into electrical and chemical energy [21, 22]. Also, new interesting applications can be found in the field of biomaterials, whose optimized surface properties are important factors enhancing bone development around medical implants. Since the formation on nanotubes is not limited to pure metals, alloys suitable for bone substitution (e.g., Ti–13Nb–13Zr) can be a subject of such surface modification. Nanostructure is used to facilitate hydroxyapatite coating and may serve as a biocompatible bridge between implants and human tissue [23–25].

The road leading to the synthesis of zirconia nanotubes started with the work of Jeon and Hwang [26] who used anodization process to prepare a zirconium oxide film which can be used as a gate dielectric material. They applied 0.1 M ammonium tartrate solution of pH=6.7. The obtained oxide films were nonporous and dense. AMF study revealed that during the anodization process, the change in surface morphology took place. At the initial stage, a significant increase

M. Stępień (✉) · P. Handzlik · K. Fitzner
Faculty of Non-Ferrous Metals, AGH University of Science and Technology, 30 Mickiewicza Avenue, 30-059 Kraków, Poland
e-mail: mstepien@agh.edu.pl

of surface roughness was observed, while further anodization lead to a reduction in surface roughness. It was suggested that ZrO_2 prepared by anodization grows by an island growth mechanism. Consequently, Tsuchiya et al. demonstrated a simple electrochemical approach to form a nanotubular zirconia layer [27, 28]. Then, in order to control the microstructure and morphology of ZrO_2 layer being formed, the influence of a number of experimental parameters as a composition of the electrolyte [29–31], applied potential [32, 33], anodization time [32], sweeping rate [30], or pH [30, 32] was investigated. Also, aqueous and nonaqueous electrolytes were applied [4, 6, 27, 28, 33, 34].

The obtained results suggest that the mechanism of self-organization of ZrO_2 nanotubes on zirconium seems to be similar to that suggested for titanium [35, 36], though, probably, a more sophisticated approach is needed to model this electrochemical process [37]. Muratore et al. [38, 39] and Fang et al. [34] pointed out the possible influence of compact and thin fluoride-rich layer formed during anodization on the tubular structure formation.

It seems that there are limits of the parameter space (voltage, pH, electrolyte, composition, etc.) in which a self-ordered structure can be formed. In this work, attempts have been made to obtain nanotubes arrays in more acidic solutions than the ones used so far and to derive tube diameter vs. voltage dependence. The influence of organic component addition on the formation of nanotubes array was also investigated.

Experimental

Zirconium foils (99.5 % purity, 1.0 mm thick, Alfa Aesar) were degreased by ultrasonic cleaning in acetone. This procedure was followed by rinsing with deionized water and electropolishing. The electrolyte used in this process was a mixture of C_2H_5OH and $HClO_4$ (volume ratio=10:1), while the operating voltage was kept constant at 16 V. During electropolishing, the solution was stirred using a mechanical stirrer (750 rpm) and kept at a constant temperature of 273.15 K. After electropolishing, the sample was rinsed with deionized water and dried in airstream. The electrochemical cell consisted of a two-electrode configuration with platinum sheet as the counter electrode and zirconium as the working electrode (the schematic cell arrangement is shown in Fig. 1). All anodization experiments were carried out at room temperature with mechanical stirring (200 rpm). During the experiments, the solution consisted of 0.1 M HF and 0.5 M Na_2SO_4 with variable glycerol addition in the range from 0 to 50 vol%. All electrolytes were prepared from analytical grade chemicals (manufactured by POCH) and deionized water. To avoid potential shock, anodic voltage was applied starting from an open circuit potential (OCP) to set point with a sweep rate of 1 V/s and then was kept constant. After the anodizing process

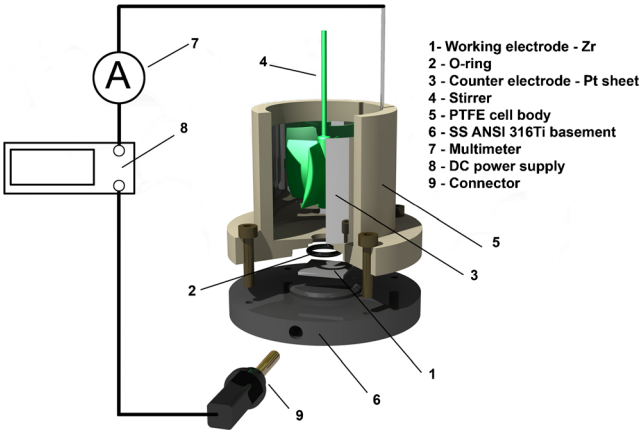

Fig. 1 Setup of the electrochemical cell

was completed, the sample was removed from the electrochemical cell and sonically cleaned in deionized water and ethanol and then dried in airstream. For electrochemical measurements, an Agilent N5751A Programmable DC Power Supply with a Keithley 2100 digital multimeter was used.

The morphology of the anodized samples was investigated by using scanning electron microscopy (SEM) Hitachi SU-70. Structural analysis of nanotubes layers was carried out with an X-ray diffractometer (Rigaku MiniFlex II) using monochromatic Cu Kα radiation (0.15416 nm). After the characterization using SEM and X-ray diffraction (XRD) techniques samples were annealed at 450 °C to check the influence of thermal treatment on morphology and structure of the nanotube layer. After annealing, samples were studied once again using the XRD method. All samples were studied by using an energy-dispersive spectroscopy (EDS) analysis (Thermo Scientific) attached to the SEM to obtain chemical composition of nanotubular layer.

Results

Inorganic solution

As a result of anodization in aqueous solutions at constant room temperature, the structure of nanotubes was obtained in the entire voltage range with the exception of 5 V in which case a nanocrystal structure of the size below 50 nm was formed. Figure 2 shows SEM top view of the nanotubes layer formed during anodization of zirconium from 10 to 60 V. In this voltage range, the outer tube diameter varied approximately in the range from 40 to 80 nm, while the inner tube diameter changed in the range from 15 to 55 nm. The diameter increases approximately linearly with an increasing anodization voltage, but tubes wall thickness stays almost constant and amounts to about 16 nm. The results of diameter

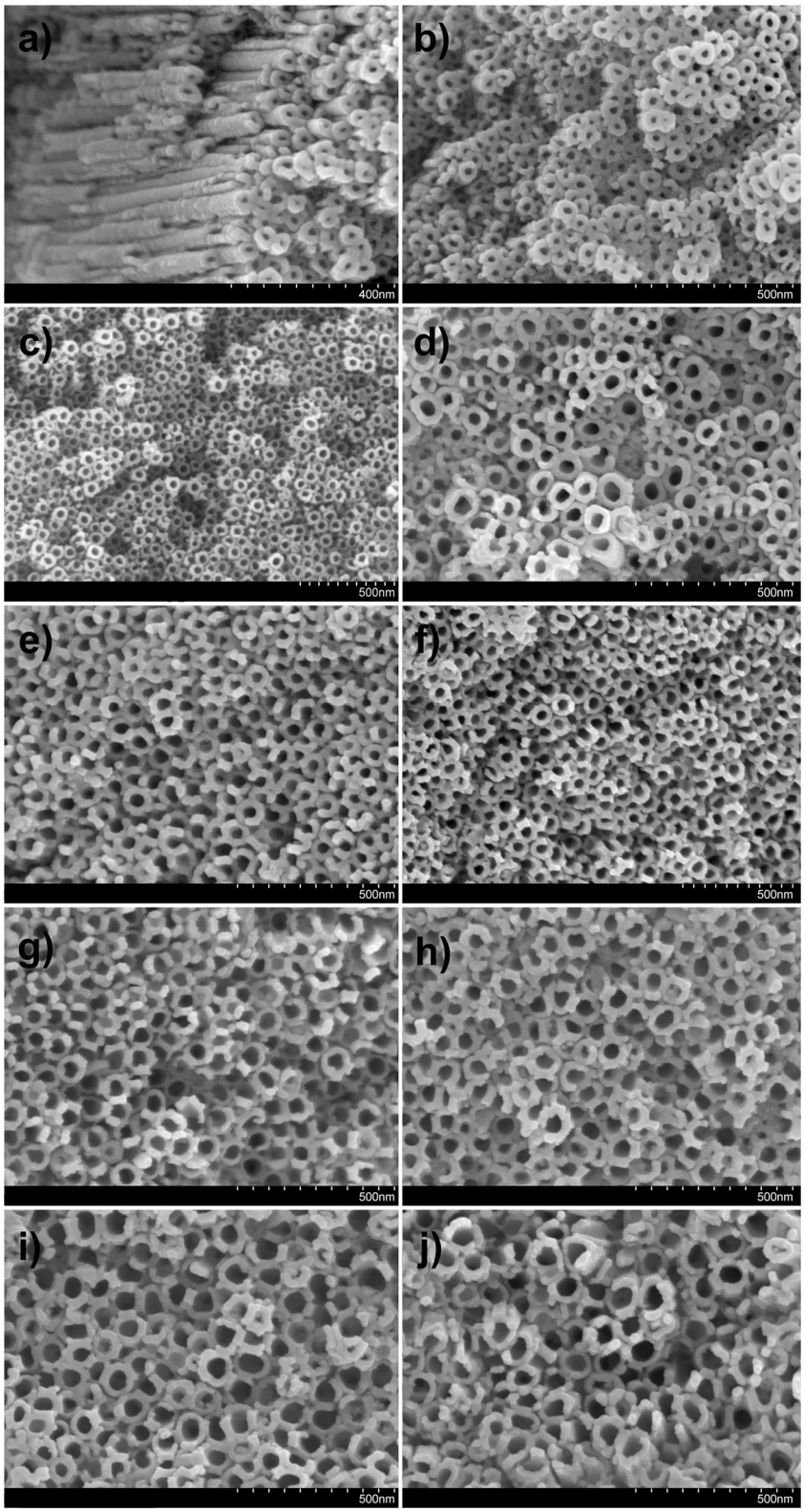

Fig. 2 SEM top views of ZrO_2 nanotubes layers anodized for 30 min in 0.1 M HF and 0.5 M Na_2SO_4 at **a** 10 V, **b** 15 V, **c** 20 V, **d** 25 V, **e** 30 V, **f** 35 V, **g** 40 V, **h** 45 V, **i** 50 V, and **j** 60 V

measurements of ZrO_2 nanotubes are shown in Fig. 3. These results support the argument that the voltage, except for fluorine ions concentration, is the most important factor influencing the morphology of the sample. We found that the increase of diameters can be described with the following linear equations:

$$d_{\text{in}}(\text{nm}) = 0.896U(\text{V}) + 7.68 \quad (1)$$

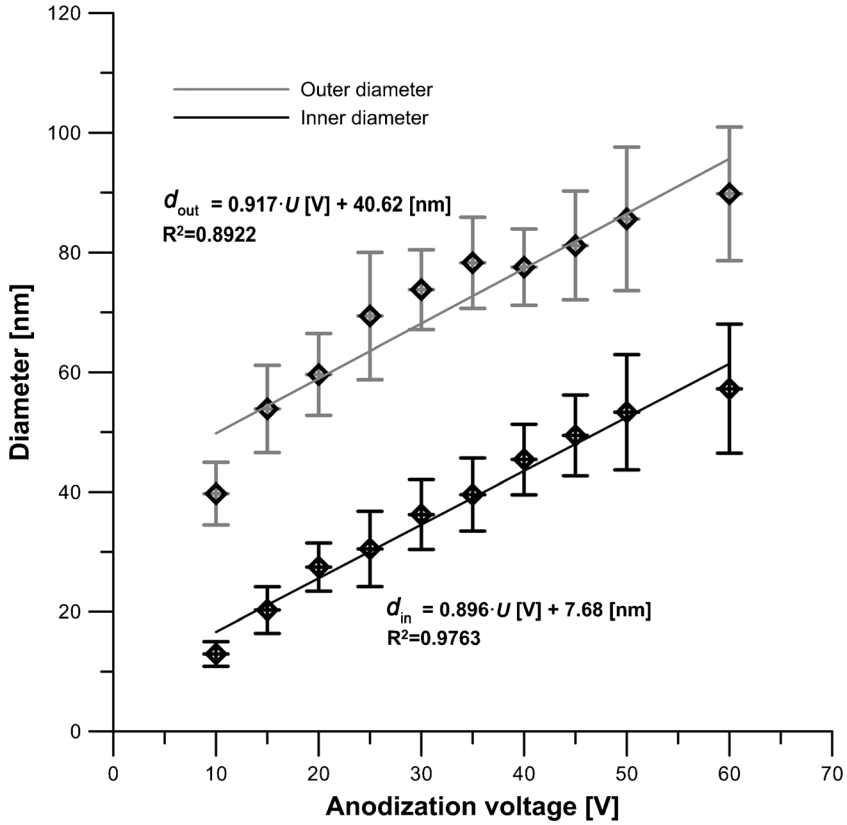

Fig. 3 The change of diameter of nanotubes with anodization voltage

$$d_{\text{out}}(\text{nm}) = 0.917U(\text{V}) + 40.62 \quad (2)$$

where d_{in} and d_{out} denote the inner and outer diameter in nanometers, and U is the anodizing voltage in volts. This dependence is shown in Fig. 3. As a measure of the order of the resulting structure, the variation coefficient of the tube diameter was assumed (the smallest coefficient of variation means highly ordered tube arrays). The coefficient of variation was calculated using the following equation:

$$C_{\text{v}} = \frac{\sigma}{\mu} \quad (3)$$

where σ is the tube diameter standard deviation, and μ is the mean tube diameter. In all cases, statistical sample size equals 50 diameter measurements.

The smallest coefficient of variation was found for the anodizing voltage equal to 20 V (see Table 1). This sample was also found to be of the best quality (Fig. 2c) without gaps between the tubes, smooth top edges, and with the shape closest to a circular cross section. Surface faults visible in Fig. 2 were formed during the mechanical removal of the top layer from the surface using ultrasonic cleaner. However, the dependence of variation coefficient with the voltage is irregular, as shown in Table 1.

The layer thickness of resulting oxide nanotubes was found to be about 10 μm for the constant anodization time of 30 min and was independent of the anodization voltage. To obtain longer nanotubes, we extend the anodization time up to 24 h for the anodization voltage equal to 20 V (the best results). The tube length increases linearly with the anodization time, but the tube diameter is in fact time-independent. However, after 5 h and with oxide layer thickness exceeding 30 μm, tubes started to collapse, and the oxide layer become very fragile. Obtained layer thickness corresponds to that reported by Tsuchiya et al. [40].

Organic electrolytes

The formation of longer nanotubes with high aspect ratio in aqueous electrolyte is difficult to achieve since after reaching certain critical length, the nanotubes collapse. Longer tubes

Table 1 Variation coefficient calculated for different nanotube structures

Anodization voltage (V)	10	15	20	25	30	35	40	45	50	60
Variation coefficient of inner diameter	0.1594	0.1918	0.1368	0.2067	0.1610	0.1540	0.1395	0.1397	0.1809	0.1883
Variation coefficient of outer diameter	0.1315	0.1355	0.0945	0.1532	0.0905	0.0975	0.1023	0.1118	0.1400	0.1243

can be obtained using organic electrolytes based on either glycerol or ethylene glycol. For the optimized anodizing voltage of 20 V, we have investigated the influence of glycerol additives on the change of shape and length of the obtained nanotubes. We carried out the process of anodization in water+glycerol solutions by a solution concentration varying from 0 to 50 vol% of glycerol addition. Figure 4 shows SEM images of nanotubes obtained in organic electrolytes.

Glycerol addition to the electrolyte slightly disturbs the order of obtained oxide nanostructure (see Fig. 4a–c) and strongly slows down the oxide layer growth rate. For optimized process parameters, if glycerol addition was more than 20 vol%, tubes did not form before 60 min of anodization. Moreover, if glycerol addition equals 50 vol%, the anodization time necessary to obtain nanotubes extends to 5 h. The influence of the process duration and glycerol addition on the oxide thickness (tubes length) and the electric charge passed is shown in Fig. 5. It is seen that glycerol addition changed tube length growth rate as a function of anodization time from linear to logarithmic. In our case, 25 vol% glycerol addition with anodization time up to 24 h let us increase the tube length (Fig. 5), but after such a long time of anodization, the nanotubes started to be disordered. Nonetheless, Fig. 4d demonstrates that while, for an aqueous electrolyte, nanotube structure cannot be formed above certain thickness, in nonaqueous electrolytes, a much thicker layer can be formed provided that the time of anodization is longer. Collapse of the tubes is not observed.

X-ray diffraction studies revealed that all nanostructured layers produced in the present work had a crystalline structure. The examples of XRD patterns of the anodized samples and the annealed samples are shown in Fig. 6. In the case of only anodized samples, the peaks correspond to metallic substrate hexagonal Zr (JCPDS card no. 00-005-0665) and to tetragonal ZrO_2 phase (JCPDS card no. 01-070-7301) in both types of electrolytes—inorganic and with addition of glycerol. This result is in agreement with some previous work where the tetragonal structure was also observed [6]. The chemical composition of the obtained ZrO_2 nanotubes was checked using an EDS analysis, and the examples of the results are presented in Fig. 7. It can be seen that the nanostructures produced only by anodization contain F^- ions (Fig. 7c), while nanotubes additionally annealed are residual fluoride-free (Fig. 7d).

The observed crystalline structure is noteworthy because nanotubes arrays formed on other valve metals such as Ti and W typically have an amorphous structure. In the case of zirconia nanotubes, the amorphous structure limits their applications area as a catalyst and photocatalyst [34]. Amorphous structure demonstrates the lack of stability in a solution of low pH level. In order to convert the amorphous structure into crystalline structure, it is necessary to apply heat treatment. The nanotubes obtained in this work do not need annealing to transform structure, which may be an important advantage in applications in which they are sensitive to thermal treatment [30]. Annealing helped to remove residual fluoride. After annealing at 450 °C, the structure of ZrO_2

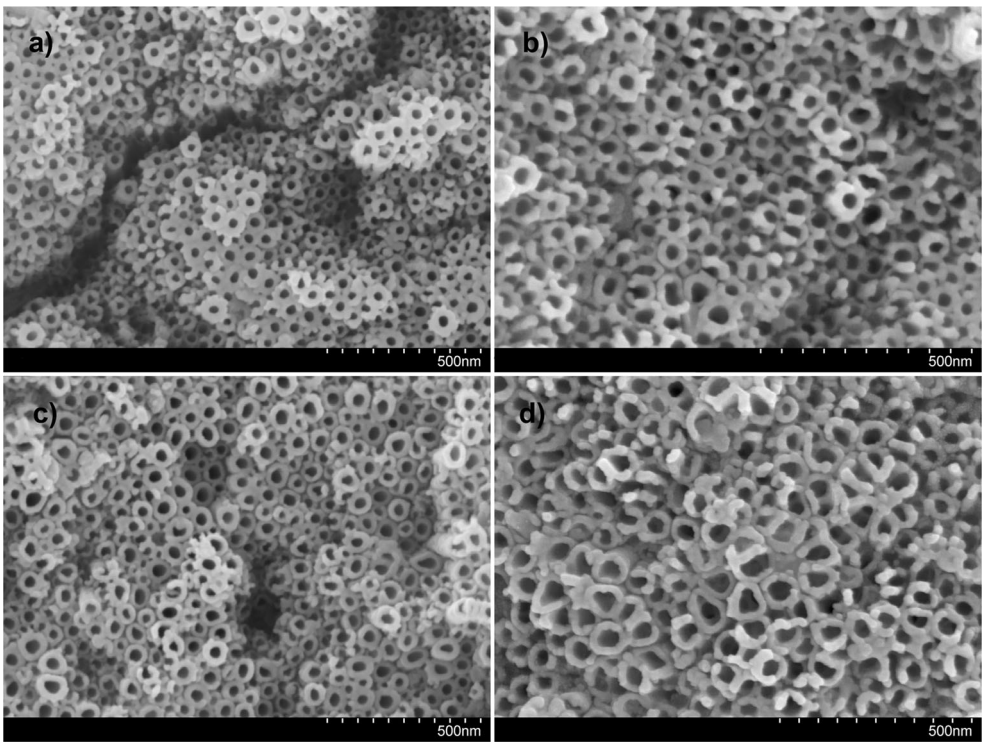

Fig. 4 SEM top views of ZrO_2 layers anodized in 0.1 M HF and 0.5 M H_2SO_4 at 20 V with **a** 5 vol% glycerol for 1 h, **b** 10 vol% glycerol for 1 h, **c** 25 vol% glycerol for 5 h, and **d** 25 vol% for 24 h

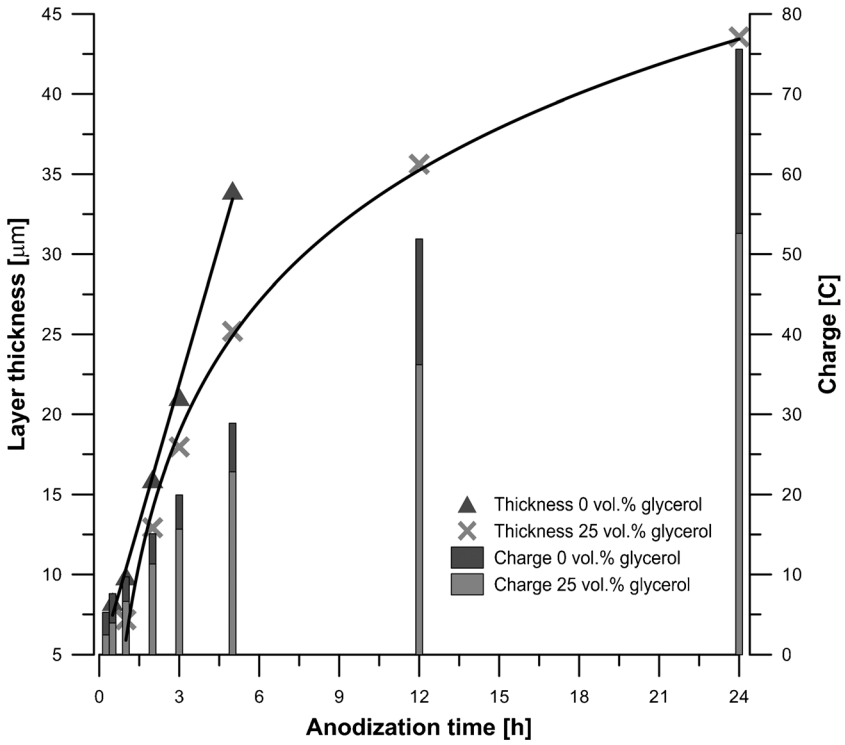

Fig. 5 Layer thickness and electric charge vs. anodization time for nanotubular arrays grown at 20 V in 0.1 M HF and 0 vol% M Na_2SO_4 without glycerol and with 25 vol% glycerol addition

changed. The main peaks of monoclinic ZrO_2 (JCPDS card no. 01-070-8739) phase appeared at 2θ=24.05°, 24.46°, 28.19°, 31.45°, and 34.09°. Some peaks of tetragonal ZrO_2 transformed into monoclinic ZrO_2, and these phases coexist together. In conclusion, ZrO_2 layers on annealed samples are composed of tetragonal and monoclinic phases, which is in accordance with the works of Zhao et al. [41] and Fang et al. [42].

Discussion

In the present work, zirconia nanotubes were formed in the electrolyte containing 0.5 M Na_2SO_4 and 0.1 M HF by direct anodization of zirconium electrode. Experiments were conducted at a constant room temperature in the solution based on HF, not on fluoride addition, which set pH of the electrolyte at the level of approximately 2.5. This is probably the reason

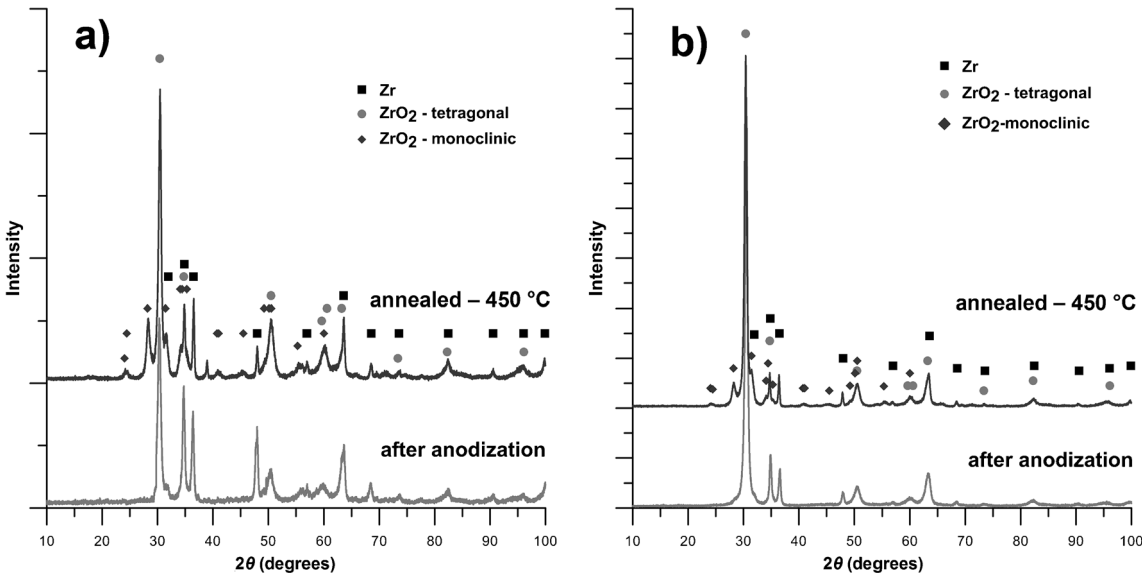

Fig. 6 XRD spectra of as-prepared and annealed at 450 °C ZrO_2 nanotubes obtained at 20 V **a** 5 h without glycerol and **b** 24 h with 25 vol% glycerol addition

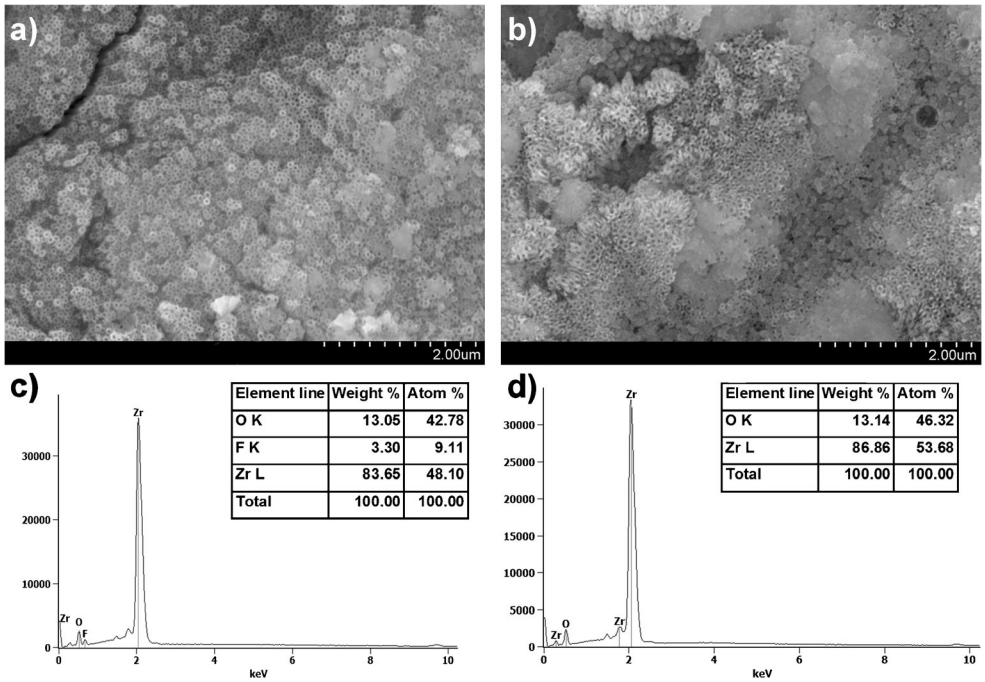

Fig. 7 **a** SEM image corresponding to EDS spectrum and analysis result (**c**) of ZrO_2 nanotubes obtained at 20 V in aqueous solution 0.1 M HF and 0.5 M H_2SO_4. **b** SEM image corresponding EDS spectrum and analysis result (**d**) of ZrO_2 nanotubes obtained at 20 V in organic solution 0.1 M HF and 0.5 M H_2SO_4 with 25 vol% glycerol addition after heat treatment at 450 °C

why diameters of the obtained nanotubes are smaller compared to those with the other studies. We varied the anodization voltage from 10 to 60 V, and we found that in this range, the outer diameter can reach 80 nm. Based on the obtained results, the linear dependence between tube diameter and anodization voltage was derived, which is shown in Fig. 3. The presented methodology used for the formation of nanotubular structure is effective and lets the size of the tubes be controlled in a one-step process without any pretreatment, which is its real advantage.

As a measure of the order of the resulting structure, the variation coefficient of the tube diameter was introduced (Eq. 3). However, the dependence of this coefficient on the voltage is irregular. Small coefficients, approximately equal to 0.13 for inner diameter, were obtained for voltages 20, 40, and 45 V. For the sample obtained with anodizing voltage equal to 25 V (Fig. 2d), large differences between nanotubes are produced. In this case, the coefficient was found to be 0.2, and it was more than 30 % larger than the one found for the tubes formed under 20 V. The increase of the voltage above 25 V reduced again the coefficient of variation as well as the differences between tubes (Fig. 2e–h). Another increase of the voltage up to 50 V results again in the increase of the coefficient of variation (Fig. 2i–j). It demonstrates that the change of variation coefficient with the anodizing voltage is nonlinear, which makes the prediction of the surface morphology difficult. A possible explanation of this erratic C_v behavior can be inferred from the results of experiments conducted in organic electrolyte. Due to its higher viscosity, all transport processes in the electrolyte are slowed down. Consequently, the anodization process in the presence of glycerol slows down. It can be inferred from current density vs. time dependence recorded during the anodization process (Fig. 8). Observed oscillations

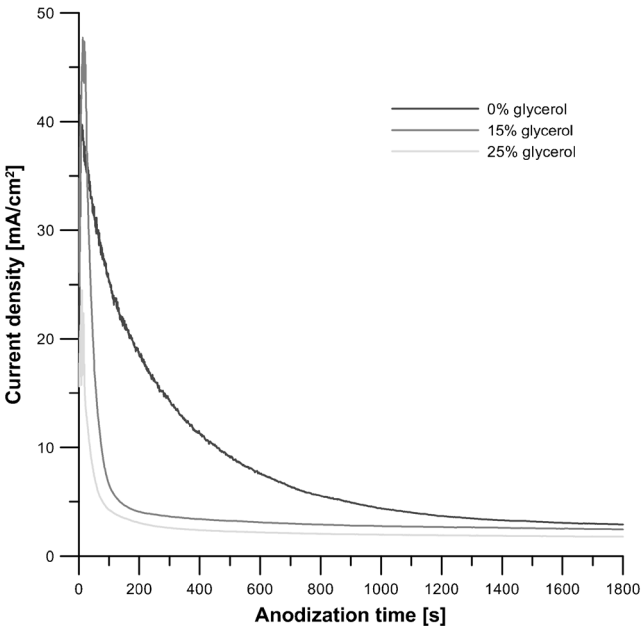

Fig. 8 Current–time curves recorded during electrochemical anodization of Zr in 0.1 M HF and 0.5 M Na_2SO_4 from OCP to 20 V (sweep rate 1 V/s) for different glycerol additions

on current density vs. time curves during the first minute can be attributed to the formation of pits which induce initiation of pores. Without glycerol, formation of pits is connected with slow current drop with oscillations (due to the change of surface electrode area), while with glycerol additions, one can see rapid current drop without oscillations. In this case, the electrolyte cannot penetrate just formed pits so fast, and the current drop is connected with increasing barrier layer thickness. Consequences of this process are shown in Fig. 5. Experiments conducted with glycerol, which took longer time, revealed that the rate of layer thickness growth varies in nonlinear fashion. Dependence of layer thickness on time indicates a logarithmic behavior. Slower growth rate observed at longer time results from enhanced chemical etching in acidic solution and simultaneously retarded oxygen diffusion in the electrolyte. As a result, faster formation of fluoride-rich matrix is followed by its dissolution.

A competition of transport vs. etching may also explain an erratic behavior of the variation coefficient in aqueous electrolyte. At higher voltage, outward-migrating Zr^{4+} ions are probably ejected into the electrolyte by field-assisted dissolution process and are not consumed in oxide formation reaction. Consequently, upper tubular layer may be a subject of the dissolution process during anodization, thus decreasing the variation coefficient.

It took a significant number of experiments to reveal the mechanism of the oxide layer growth. Tsuchiya et al. [27, 28, 40] demonstrated a simple approach to form a nanotubular layer by using H_2SO_4+NaF electrolyte with pH=0.15. The pores showed an irregular morphology with a diameter equal to approximately 50 nm and layer thickness up to 40 μm after 5 h of anodization. The formation of smooth and straight nanotubes was achieved in the subsequent work [43], in which 1 M $(NH_4)_2SO_4$+0.5 wt% NH_4F with pH=5.3 electrolyte was used under a constant potential of 20 V. Further investigations showed [30] that the potential sweep rate from the OCP to anodizing potential can be an important factor to fabricate self-organized nanotube layers. From the results of the above investigations, it can be deduced that fluoride ions in the solution are necessary to induce competing chemical dissolution of the oxide, while the morphology and the structure of the deposit can be influenced by pH, electrolyte composition, and imposed potential.

Optimizing further the anodization process, Berger et al. [5] used two different surface pretreatment processes which improved the growth and morphology of the resulting nanotube arrays. Nanotube diameter equals 60 nm, and their length is between 3 and 40 μm with anodization time in the range from 1 to 24 h. Experiments were done in 1 M $(NH_4)SO_4$ electrolyte with the addition of NH_4F with pH=5.3. It was observed that the chemical dissolution under more acidic conditions took place, resulting in a decay of the surface structure. Changing the electrolyte, Ismail et al. [6] carried out the anodization of Zr foil in Na_2SO_4+NH_4F solution at the voltage of 20 V. Oxide film with nanotubular structure was obtained, but an increase in voltage disrupted the self-ordering of the anodic layer at the thickness of about 6 μm. It can be speculated that the distribution of electric field in zirconia is related to surface morphology fluctuation. As a result, field-assisted dissolution may occur resulting in the formation of pits, which are pore nucleation centers, and in the presence of F^- ions, their attack on pits takes place. However, no attempts have been made to correlate the diameter of tubes with the voltage by functional dependence.

It has already been reported that using the organic additives such as glycerol or ethylene glycol will usually either increase the thickness of the layer or change the order of its structure [27, 28, 44]. Berger et al. [5, 44] used ethylene glycol/glycerol-based electrolyte added to NH_4F aqueous solution and observed a significant increase of the oxide layer thickness. Moreover, by varying the water addition, they managed to demonstrate the switch between porous and tubular morphology. It was also found that the increase of the layer thickness follows at a much slower rate than that in the aqueous solution, but the collapse of the obtained layer takes place for much longer tubes.

The mechanism of tubular structure formation has been not quite clear. Khalil and Leach [29] pointed out that a variety of species from acidic electrolyte can be incorporated into oxide layer. They evaluated the effect of F^- ions on the growth behavior of the oxide layer. They found that the incorporation of fluoride ions into oxide structure promotes either amorphous or microcrystalline oxide formation. When sufficient concentration of fluoride ions is added, a breakdown of the oxide film takes place.

Porous film formation in glycerol+fluoride electrolyte with different water additions was examined by Muratore et al. [39]. It was demonstrated that the initial films formed on the metal surface contain a significant amount of fluorine. Water addition reduces the fluorine content of the film and increases oxygen content. It seems that under applied potential, ionic migration takes place within the oxide layer with F^- ions migrating inward faster than O^{2-} ions, leading to fluoride-rich layer between nanotubes and metal–film interface. Since a loss of fluorine is observed during immersion in the electrolyte, the dissolution process must take place, resulting in separation of cells.

Also, Vacandio et al. [32] studied the influence of the electrolyte composition upon layer morphology. In this study, four different compositions of the electrolyte with pH level between 3 and 6 were used. It was found that a fluoride-containing electrolyte exhibits a higher current density which may indicate growing pores at the metal–electrolyte interface. Water addition to the electrolyte changed the surface morphology. Assuming that fluoride ions are expected to act as

dissolution agents forming soluble metal–fluoro complexes, they suggested a set of reactions leading to pore nucleation.

A recent study conducted by Muratore et al. [39] revealed that fluoride-rich material separates the relatively oxygen-rich nanotubes from the substrate and from each other which can be exposed due to the dissolution of fluoride-rich material. The addition of water leads to easier tube separation. In the subsequent study, Muratore et al. [38] used ammonium fluoride in glycerol to investigate the effect of aging of the oxide film in the electrolyte after anodization. They demonstrated that this process promotes the transition from porous to nanotubular morphology due to the dissolution of fluoride-rich matrix.

The effect of heat treatment on the morphology and crystalline structure of anodic ZrO_2 was investigated by Fang et al. [45]. They used formamide+glycerol electrolyte with NH_4F and H_2O additions. After anodization, the samples had an amorphous structure which could be converted to tetragonal and monoclinic modifications after heating in a temperature range of 400–900 °C. In their most recent study, Fang et al. [34] followed an architecture evolution of nanotubes at different anodization points. They showed that while after 1 h, a compact layer rich in fluorine is formed between Zr and upper tubular layer, it disappears after 3 h. These results indicate that the outer layer of ZrO_2 nanotubes is fluoride-rich, and it can be dissolved in the surrounding electrolyte.

Taking into account the results of the above investigations as well as other works concerned with Al, Ti, and Nb anodization [3, 10, 43, 46, 47], one can suggest a general scheme leading to the formation of oxide nanotubes on the metal surface. A steady state must be reached for the process in which oxide formation is nearly compensated by oxide dissolution. Depending on oxide conductivity, a mechanism of the dissolution process may be different. A steady state can be detected by recording either applied voltage vs. time at constant current density or current density vs. time at constant voltage. Characteristic plateau on these dependencies indicates formation of pores. However, it is electrolyte-dependent. In order to optimize the process, other variables like pH, composition of the electrolyte, and temperature should be adjusted. Morphology examination can show which set of parameters is a right one for self-organization of tubes. It seems that this scheme can be applied to any valve metal.

Conclusions

High-quality zirconia nanotubes layer was obtained by using the single-step direct anodization of zirconium in aqueous and nonaqueous electrolytes containing F^- ions. For the aqueous electrolyte (0.5 M Na_2SO_4+0.1 M HF) and voltage range between 10 and 60 V, morphology of nanotubes was achieved. Diameter of tubes is linearly dependent on the applied voltage (Fig. 3). Layer thickness in inorganic electrolyte increases linearly with anodization time up to 5 h, and after this time, tubes collapse. The best results were obtained for anodization voltages 20, 40, and 45 V with the process time ranging from 0.5 to 3 h. In organic electrolytes, we obtained a slightly longer layer of nanotubes of up to 44 μm, after 24 h of anodization. X-ray diffraction showed that the nanotubes produced by direct anodization and nanotubes additionally annealed exhibit a crystalline structure. After anodization, ZrO_2 nanotubes exhibit a tetragonal structure, while after annealing, monoclinic phase appeared. Comparing the nanotubes we obtained for anodizing voltage of 20 V with the results of other investigations, we can conclude that the advantage of this approach is a one-step process without any pretreatment leading to high-quality nanotubes.

References

1. Masuda H, Fukuda K (1995) Ordered metal nanohole arrays made by a two - step replication of honeycomb structures of anodic aluminia. Science 268:1466–1468
2. Grimes CA, Varghese OK et al (2001) Titanium oxide nanotube arrays prepared by anodic oxidation. J Mater Res 16(2001):3331–3334
3. Roy P, Berger S, Schmuki P (2011) TiO_2 nanotubes: synthesis and applications. Angew Chem Int Ed 50:2904–2939
4. Tsuchiya H, Macak JM, Taveira L, Schmuki P (2005) Fabrication and characterization of smooth high aspect ratio zirconia nanotubes. Chem Phys Lett 410:188–191
5. Schmuki P, Berger S (2008) Enhanced self-ordering of anodic ZrO2 nanotubes in inorganic and organic electrolytes using two-step anodization. Phys Status Solidi (RRL) 3:102–104
6. Ismail S, Ahmad ZA, Berenov A, Lockman Z (2011) Effect of applied voltage and fluoride ion content on the formation of zirconia nanotube arrays by anodic oxidation of zirconium. Corros Sci 53:1156–1164
7. Muratore F, Baron-Wiecheć A, Hashimoto T, Skeldon P, Thompson GE (2010) Anodic zirconia nanotubes: composition and growth mechanism. Electrochem Commun 12(2010):1727–1730
8. Choi J, Lim JH, Lee SC, Chang JH, Kim KJ, Cho MA (2006) Porous niobium oxide films prepared by anodization in HF/H_3PO_4. Electrochim Acta 51:5502–5507
9. Habazaki H, Oikawa Y, Fushimi K, Aoki Y, Shimizu K, Skeldon P, Thompson GE (2009) Importance of water content in formation of porous anodic niobium oxide films in hot phosphate-glycerol electrolyte. Electrochim Acta 54:946–951
10. Wei W, Lee K, Shaw S, Schmuki P (2012) Anodic formation of high aspect ratio, self-ordered Nb_2O_5 nanotubes. Chem Commun 48:4244–4246
11. Kim H-W, Lee S-Y, Bae C-J, Noh Y-Y, Kim H-E, Kim H-M, Ko JS (2003) Porous ZrO_2 bone scaffold coated with hydroxyapatite with fluorapatite intermediate layer. Biomaterials 24:3277–3284

12. Minagar S, Berndt CC, Wang J, Ivanowa E, Wen C (2012) A review of the application of anodization for the fabrication on nanotubes on metal implant surfaces. Acta Biomater 8:2875–2888
13. Zhang Q, Shen J, Wang J, Wu G, Chen L (2000) Sol–gel derived ZrO_2–SiO_2 highly reflective coatings. Int J Inorg Mater 2:319–323
14. Ivers-Tiffee E, Hardtl KH, Menesklou W, Riegel J (2001) Principles of solid state oxygen sensor for lean combustion gas control. Electrochim Acta 47:807–814
15. Lu G, Miura N, Yamazoe N (2000) Stabilized zirconia-based sensor using WO_3 electrode for detection of NO or NO_2. Sensors Actuators B Chem 65:125–127
16. Ahmed AI, El-Hakam SA, Samra SE, El-Khouly AA, Khder AS (2008) Structural characterization of sulfated zirconia and their catalytic activity in dehydration of ethanol. Colloids Surf A Physicochem Eng Asp 317:62–70
17. Jin G, Lu G, Guo Y, Guo Y, Wang J, Kong W, Liu X (2005) Effect of preparation condition on performance of Ag–MoO_3/ZrO_2 catalyst for direct epoxidation of propylene by molecular oxygen. J Mol Catal A Chem 232:165–172
18. Cao W, Tan OK, Zhu W, Jiang B, Gopal RC (2001) An amorphous-like xa-Fe_2O_3-$(1-x)ZrO_2$ solid solution system for low temperature resistive-type oxygen sensing. Sensor Actuators B 77:421–426
19. Cho HJ, Choi GM (2008) Effect of milling methods on performance of Ni–Y_2O_3-stabilized ZrO_2 anode for solid oxide fuel cell. J Power Sources 176:96–101
20. Zhang QH, Li Y, Xu B-Q (2004) Reforming of methane and coalbed methane over nanocomposite Ni/ZrO_2 catalyst. Catal Today 98:601–605
21. Evanoff DD, Chumanov G (2005) Synthesis and optical properties of silver nanoparticles and arrays. Eur J Chem Phys Phys Chem 6:1221
22. Chandersekharan N, Kamat PV (2000) Improving the photoelectrochemical performance of nanostructured TiO_2 films by adsorption of gold nanoparticles. J Phys Chem B 104:10851–10857
23. Geetha M, Singh AK, Asokamani R, Gogia AK (2009) Ti based biomaterials, the ultimate choice for orthopedic implants—a review. Prog Mater Sci 54:397–425
24. Cvijovic-Alagic I, Cvijovic Z, Mitrovic S, Panic V, Rakin M (2011) Wear and corrosion behaviour of Ti–13Nb–13Zr and Ti–6Al–4V alloys in simulated physiological solution. Corros Sci 53:796–808
25. Narayanan R, Lee H-J, Kwon T-Y, Kim K-H (2011) Anodic TiO_2 nanotubes from stirred bath: hydroxyapatite growth & osteoblast responses. Mater Chem Phys 125:510–517
26. Jeon S, Hwang H (2003) Electrical characteristics of ZrO_2 prepared by electrochemical anodization of Zr in an ammonium tartrate electrolyte. J Vac Sci Technol A 21:L5
27. Tsuchiya H, Macak JM, Sieber I, Schmuki P (2005) Self-organized high-aspect-ratio nanoporous zirconium oxides prepared by electrochemical anodization. Small 7:722–725
28. Tsuchiya H, Macak JM, Sieber I, Schmuki P (2006) Anodic porous zirconium oxide prepared in sulfuric acid electrolytes. Mater Sci Forum 512:205–210
29. Khalil N, Leach JSL (1996) Anodic oxidation of zirconium: effect of fluoride contamination on oxide structure and transport processes. J Appl Electrochem 26:231–233
30. Tsuchiya H, Macak JM, Ghicov A, Taveira L, Schmuki P (2005) Self-organized porous TiO_2 and ZrO_2 produced by anodization. Corros Sci 47:3324–3335
31. Pauporte T, Finne J (2006) Impedance spectroscopy study of anodic growth of thick zirconium oxide films in H_2SO_4, Na_2SO_4 and NaOH solutions. J Appl Electrochem 36:33–41
32. Vacandio F, Eyraud M, Chassigneux C, Knauth P, Djenizian T (2010) Electrochemical synthesis and characterization of zirconia nanotubes grown from Zr thin films. J Electrochem Soc 157(12):K279–K283
33. Muratore F, Baron-Wiecheć A, Gholinia A, Hashimoto T, Skeldon P, Thompson GE (2011) Comparison of nanotube formation on zirconium in fluoride/glycerol electrolytes at different anodizing potentials. Electrochim Acta 58:389–398
34. Fang D, Yu J, Luo Z, Liu S, Huang K, Xu W (2012) Fabrication parameter-dependent morphologies of self-organized ZrO_2 nanotubes during anodization. J Solid State Electrochem 16:1219–1228
35. Yasuda K, Macak JM, Berger S, Ghicov A, Schmuki P (2007) Mechanistic aspect of the self-organization process for oxide nanotube formation on valve metals. J Electrochem Soc 154(9):C472–C478
36. Schmuki P, Virtanen S (2009) Electrochemistry at the nanoscale. Nanostructured Science and Technology. New York. doi:10.1007/978-0-387-73582-5
37. Krischer K (2001) Spontaneous formation of spatiotemporal patterns at the electrode electrolyte interface. J Electroanal Chem 501:1–21
38. Muratore F, Hashimoto T, Skeldon P, Thompson GE (2011) Effect of ageing in the electrolyte and water on porous anodic films on zirconium. Corros Sci 53:2299–2305
39. Muratore F, Baron-Wiechec A, Hashimoto T, Gholinia A, Skeldon P, Thompson GE (2011) Growth of nanotubes on zirconium in glycerol/fluoride electrolytes. Electrochim Acta 56(28):10500–10506
40. Tsuchiya H, Schmuki P (2004) Thick self-organized porous zirconium oxide formed in H_2SO_4/NH_4F electrolytes. Electrochem Commun 6:1131–1134
41. Zhao J, Wang X, Xu R, Meng F, Guo L, Li Y (2008) Fabrication of high aspect ratio zirconia nanotube arrays by anodization of zirconium foils. Mater Lett 62:4428–4430
42. Fang D, Luo Z, Liu S, Zeng T, Liu L, Xu J, Bai Z, Xu W (2013) Photoluminescence properties and photocatalytic activities of zirconia nanotube arrays fabricated by anodization. Opt Mater 35:1461–1466
43. Sieber I, Hildebrand H, Friedrich A, Schmuki P (2005) Formation of self-organized niobium porous oxide on niobium. Electrochem Commun 7:97–100
44. Berger S, Jakubka F, Schmuki P (2008) Formation of hexagonally ordered nanoporous anodic zirconia. Electrochem Commun 10:1916–1919
45. Fang D, Huang K, Luo Z, Wang Y, Liu S, Zhang Q (2011) Freestanding ZrO_2 nanotube membranes made by anodic oxidation and effect of heat treatment on their morphology and crystalline structure. J Mater Chem 21:4989
46. Yang L, Luo S, Cai Q, Yao S (2010) A review on TiO_2 nanotube arrays: fabrication, properties, and sensing applications. Chin Sci Bull 55:331–338
47. Li A-O, Birner A, Nielsch K, Gosele U (1998) Hexagonal pore arrays with a 50–420 nm interpore distance formed by self-organization in anodic alumina. J Appl Phys 84:6023